

Anomalous scaling and phase transition in large deviations of dynamical observables of stationary Gaussian processes

Alexander Valov^{1,*} and Baruch Meerson^{2,†}

¹*Instituto Balseiro, Univ. Nacional de Cuyo, Av. Bustillo, 9500, Argentina*

²*Racah Institute of Physics, Hebrew University of Jerusalem, Jerusalem 91904, Israel*

We study large deviations, over a long time window $T \rightarrow \infty$, of the dynamical observables $A_n = \int_0^T x^n(t) dt$, $n = 3, 4, \dots$, where $x(t)$ is a centered stationary Gaussian process in continuous time. We show that, for short-correlated processes the probability density of A_n exhibits an anomalous scaling $P(A_n, T) \sim \exp[-T^\mu f_n(\Delta A_n T^{-\nu})]$ at $T \rightarrow \infty$ while keeping $\Delta A_n T^{-\nu}$ constant. Here ΔA_n is the deviation of A_n from its ensemble average. The anomalous exponents μ and ν depend on n and are smaller than 1, whereas the rate function $f_n(z)$ exhibits a first-order dynamical phase transition (DPT) which resembles condensation transitions observed in many systems. The same type of anomaly and DPT, with the same μ and ν , was previously uncovered for the Ornstein-Uhlenbeck process – the only stationary Gaussian process which is also Markovian. We also uncover an anomalous behavior and a similar DPT in the *long-correlated* Gaussian processes. However, the anomalous exponents μ and ν are determined in this case not only by n but also by the power-law long-time decay $\sim |t|^{-\alpha}$ of the covariance function. The different anomalous scaling behavior is a consequence of a faster-than-linear scaling with T of the variance of A_n . Finally, for sufficiently long-ranged correlations, $\alpha < 2/n$, the DPT disappears, giving way to a smooth crossover between the regions of typical, Gaussian fluctuations and large deviations. The basic mechanism behind the DPT is the existence of strongly localized optimal paths of the process conditioned on very large A_n and coexistence between the localized and delocalized paths of the conditioned process. Our theoretical predictions are corroborated by replica-exchange Wang-Landau simulations where we could probe probability densities down to 10^{-200} .

I. INTRODUCTION

Fluctuations of “dynamical observables”, which describe the cumulative effect of the histories of stochastic processes over a long time window T , is an important subject of nonequilibrium statistical mechanics and probability theory [1]. Theoretical description of dynamical observables is challenging because they defy standard tools of equilibrium statistical mechanics: in particular, by exhibiting nonequilibrium behaviors even when the underlying system is in thermal equilibrium. Furthermore, in the limit of $T \rightarrow \infty$ the full probability distribution of dynamical observables – which includes large deviations [1–4] – can exhibit singularities which, by analogy with equilibrium phase transitions, are called dynamical phase transitions (DPTs).

A simple but important class of dynamical observables deals with the quantities

$$A_n = \int_0^T x^n(t) dt, \quad n = 1, 2, \dots, \quad (1)$$

where $x(t)$ is a centered stationary stochastic process. In standard cases fluctuations of these quantities obey a simple large-deviations principle where, in the limit of $T \rightarrow \infty$, the probability distribution of A behaves as

$$P(A_n, T) \sim e^{-T\Phi_n(\Delta A_n/T)}, \quad (2)$$

where ΔA_n is the deviation of A_n from its mean [5]. The rate function $\Phi_n(y)$ is usually convex, and it vanishes at $y = 0$. If the process is Markovian, $\Phi_n(y)$ can be obtained from the Donsker–Varadhan (DV) theory, where the calculations reduce to determining the largest eigenvalue of a modified (tilted) generator of the process $x(t)$; see Ref. [5] for an accessible exposition. The DV theory, however, breaks down when the spectrum of the tilted generator is not bounded from above [6–8]. As a result, an anomalous scaling

$$P(A_n, T) \sim e^{-T^\mu f_n(\Delta A_n/T^\nu)}, \quad (3)$$

* aleksandr.valov@ib.edu.ar

† meerson@mail.huji.ac.il

arises in the limit of $T \rightarrow \infty$, while keeping $\Delta A_n/T^\nu$ constant [9]. The anomalous exponents μ and ν differ from the standard values $\mu = \nu = 1$, and they depend on the specific system and on n . Anomalous scaling of this type is observed, at $n > 2$, already for the classic Ornstein-Uhlenbeck process, which describes an overdamped motion of a Brownian particle in a quadratic potential [10]. In this case one obtains [9]

$$\mu = \frac{2}{2n-2} \quad \text{and} \quad \nu = \frac{n}{2n-2}. \quad (4)$$

The anomalous scaling behavior is closely related to a change in the character of the most likely history of the process conditioned on a value of A_n : from contributions spread uniformly in time to localized, instanton-like events that produce a macroscopic contribution to A_n [6, 9, 11–13]. Remarkably, the rate function $f_n(z)$ in Eq. (3) exhibits a first-order dynamical phase transition (DPT) [9] which is similar to “condensation transitions” observed in many other settings, see e.g. [14–18]. The mechanism behind the first-order DPT is the coexistence (at different times) of two different types of the time histories of the system – delocalized and localized in time – which dominate the contribution to A_n [9]. This mechanism manifests itself in the expression for rate function $f_n(z)$ in Eq. (3) [9]:

$$f_n(y) = \min_{z \in [0, y]} F_n(y, z), \quad (5)$$

where

$$F_n(y, z) = \beta_n(y - z)^2 + c_n z^{2/n}, \quad n > 2, \quad (6)$$

where $\beta_n > 0$, $c_n > 0$, and $n = 2, 3, \dots$. The first, quadratic term on the right-hand side of Eq. (6), with

$$\beta_n \simeq \frac{T}{2\text{Var}(A_n)}, \quad (7)$$

describes the contribution of the (typical) Gaussian fluctuations of A_n around the mean $\langle A_n \rangle$. For the OU process, the variance of A_n grows as T at large T , therefore β_n is time-independent.

The second term in Eq. (6) describes the contribution of a strongly localized, instanton-like optimal path of the process which dominates the probability density of large A_n [6]. The first-order DPT appears, at $T \rightarrow \infty$, at the point

$$y = y_c = \frac{n-1}{n-2} \left[\frac{(n-2)c_n}{n\beta_n} \right]^{\frac{n}{2n-2}}, \quad n > 2, \quad (8)$$

where the first derivative of the rate function $f_n(y)$ exhibits a discontinuity.

A question naturally emerges regarding the extent to which these anomalies and DPT are universal. In particular, can they arise if the stationary process $x(t)$ is non-Markovian, so that the Feynman-Kac method – and, as a result, the DV theory – do not apply? A first step in addressing this question was taken in Ref. [12] which considered (in general non-Markovian) Gaussian stationary processes with short correlations and applied the optimal fluctuation method (OFM) to study the large deviations of A_n . For $n > 2$, the large deviations of A_n were found to exhibit the same scaling behavior, $-\ln P(A_n, T) \sim A_n^{2/n}$, independent of T , as their counterparts for the OU process. This result showed that the breakdown of the simple large-deviations principle (2), previously observed in the OU process [6], also occurs for short-correlated Gaussian processes [12].

Here we considerably extend the earlier work and study anomalous scaling and the ensuing DPT in the full probability distribution $P(A_n, T \rightarrow \infty)$ of stationary Gaussian processes: both short- and long-correlated. To remind the reader, a centered stationary Gaussian process $x(t)$ is fully determined by its covariance

$$\kappa(s) = \langle x(t)x(t+s) \rangle. \quad (9)$$

As we will see, for *short-correlated* Gaussian processes – that is, when $\kappa(t)$ decays sufficiently fast at $|t| \rightarrow \infty$ – the typical fluctuations of A_n are normally distributed with a variance growing linearly with T . This fact, combined with the $A_n^{2/n}$ scaling of the action for large A_n [12], implies that, for such processes, the probability distribution of A_n for $n > 2$ obeys an anomalous scaling of the type (3), with the same exponents μ and ν [given by Eq. (4)] as for the OU process. Furthermore, here too the rate function $f_n(z)$ is described by Eqs. (5) and (6) (with coefficients determined by the covariance of the particular Gaussian process), and it exhibits a first-order DPT of the same type.

We will also show here that a similar first-order DPT can exist, under certain conditions, for *long-correlated* Gaussian processes. In this case, however, the exponents μ and ν are determined not only by n , but also by the long-time power-law tail of the covariance.

Furthermore, we show that, when the correlations are too long-ranged, the DPT disappears, giving way to a smooth crossover between the regions of typical, Gaussian fluctuations and large deviations. Overall, we obtain a phase diagram which shows regions of different behavior of the anomalous exponents μ and ν [see Eq. (3)] and the presence or absence of the DPT in the rate function $f_n(y)$. Our general results are illustrated on several particular examples of stationary Gaussian processes. These include the fractional Ornstein-Uhlenbeck process [19, 20], where by varying the Hurst exponent H , one can observe all the three regimes of anomalous behavior described above. Finally, we corroborate our analytical predictions numerically by using replica-exchange Wang-Landau simulations, which allow us to measure probabilities as small as 10^{-200} . Our numerics includes the important case $H = 1/2$ (the standard OU process), for which the theoretical predictions (3)-(8) [9] have so far not been tested numerically.

The layout of the remainder of the paper is the following. In Sec. II we present our results for the short-correlated systems. The long-correlated systems are dealt with in Sec. III. Our large-deviation simulations and verification of our theoretical predictions are described in Sec. IV. We summarize and briefly discuss our results in Sec. V.

II. SHORT-CORRELATED GAUSSIAN PROCESSES

A. Typical fluctuations of A_n

The typical fluctuations of A_n around the mean follow the Gaussian distribution,

$$P(A_n, T) \simeq P_{\text{Gauss}}(A_n, T) = \frac{1}{\sqrt{2\pi\text{Var}_n}} \exp \left[-\frac{(A_n - \langle A_n \rangle)^2}{2\text{Var}_n} \right], \quad (10)$$

where Var_n is the variance of A_n , and

$$\langle A_n \rangle = \int_0^T \langle x^n(t) \rangle dt = T \frac{[1 + (-1)^n][2\kappa(0)]^{n/2} \Gamma(\frac{n+1}{2})}{2\sqrt{\pi}}. \quad (11)$$

Obviously $\langle A_n \rangle$ is nonzero only for even n . The second moment of A_n can be written as

$$\langle A_n^2 \rangle = \int_0^T \int_0^T \langle x^n(t) x^n(s) \rangle dt ds. \quad (12)$$

The covariances $\langle x^n(t) x^n(s) \rangle$ can be evaluated either with the help of the bivariate normal distribution or, more conveniently, via Isserlis-Wick theorem [21]. For any stationary Gaussian process and arbitrary $n = 1, 2, \dots$, Isserlis-Wick's theorem reduces this covariance to a finite sum over powers of pairwise covariances:

$$\langle x^n(t) x^n(s) \rangle = \sum_{m=0}^{\lfloor \frac{n}{2} \rfloor} \frac{(n!)^2}{(n-2m)!(2^m m!)^2} \kappa^{2m}(0) \kappa^{n-2m}(t-s), \quad (13)$$

where $[z]$ is the integer part of z . Substituting Eq. (13) into Eq. (12) and subtracting the squared mean (11), we obtain a general expression for the variance of A_n (we denote it as Var_n) for an arbitrary stationary Gaussian process and for any n :

$$\text{Var}_n = \sum_{m=0}^{\lfloor \frac{n-1}{2} \rfloor} \frac{(n!)^2}{(n-2m)!(2^m m!)^2} \kappa^{2m}(0) \int_0^T \int_0^T \kappa^{n-2m}(t-s) dt ds. \quad (14)$$

Crucially, for short-correlated processes the $T \rightarrow \infty$ asymptotic of Var_n is proportional to T , because in this case

$$\int_0^T \int_0^T \kappa^{n-2m}(t-s) dt ds \simeq T \int_{-\infty}^{\infty} \kappa^{n-2m}(z) dz. \quad (15)$$

As a result, the coefficient β_n in Eq. (7) is T -independent, which is a pre-requisite for the validity of Eqs. (5) and (6). Let us illustrate Eq. (14) on two particular examples of Gaussian processes.

1. OU covariance

The OU process is the only process (up to a simple rescaling) that is both Gaussian, and Markovian. By rescaling t and x , we can choose its covariance to be parameter-free: $\kappa(t) = (1/2) \exp(-|t|)$. Using Eq. (14), we can calculate the $T \gg 1$ asymptotic of the variance of A_n for arbitrary n . The result,

$$\text{Var}_n^{\text{OU}} \simeq T \sum_{m=0}^{\lfloor \frac{n-1}{2} \rfloor} \frac{(n!)^2}{(n-2m)(n-2m)! 2^{n+2m-1} (m!)^2}, \quad (16)$$

is equivalent to Eq. (14) of Ref. [11]. In particular, for $n = 3, 4, 5$ and 6 Eq. (16) yields

$$\begin{cases} \text{Var}_3^{\text{OU}} \simeq \frac{11}{4}T, & \beta_3 = \frac{2}{11}, \\ \text{Var}_4^{\text{OU}} \simeq \frac{21}{4}T, & \beta_4 = \frac{2}{21}, \\ \text{Var}_5^{\text{OU}} \simeq \frac{449}{16}T, & \beta_5 = \frac{8}{449}, \\ \text{Var}_6^{\text{OU}} \simeq \frac{3495}{32}T, & \beta_6 = \frac{16}{3495}. \end{cases} \quad (17)$$

where we used Eq. (7) to determine the coefficients β_n . For $n = 3$ and 4 these results coincide with those obtained perturbatively within the framework of the DV theory [9]. Equation (16) allows one to easily obtain β_n for arbitrarily large n , where the perturbative quantum-mechanical calculations [9] require a bit more technical effort.

2. Gaussian covariance

Our second example deals with a centered stationary Gaussian process with a Gaussian covariance. Again, by rescaling t and x we can choose the covariance to be parameter-free: $\kappa(t) = \exp(-t^2)$. Plugging this covariance into Eq. (14), we obtain the $T \gg 1$ asymptotic of the variance of A_n :

$$\text{Var}_n^{\text{Gauss}} \simeq \sqrt{\pi} T \sum_{m=0}^{\lfloor \frac{n-1}{2} \rfloor} \frac{(n!)^2}{\sqrt{n-2m} (n-2m)! 2^{2m} (m!)^2}. \quad (18)$$

For $n = 3, 4, 5$ and 6 Eqs. (18) and (7) yield

$$\begin{cases} \text{Var}_3^{\text{Gauss}} \simeq (9 + 2\sqrt{3})\sqrt{\pi}T, & \beta_3 = \frac{1}{2(9+2\sqrt{3})\sqrt{\pi}}, \\ \text{Var}_4^{\text{Gauss}} \simeq 12(1 + 3\sqrt{2})\sqrt{\pi}T, & \beta_4 = \frac{1}{24(1+3\sqrt{2})\sqrt{\pi}}, \\ \text{Var}_5^{\text{Gauss}} \simeq (225 + 200\sqrt{3} + 24\sqrt{5})\sqrt{\pi}T, & \beta_5 = \frac{1}{2(225+200\sqrt{3}+24\sqrt{5})\sqrt{\pi}}, \\ \text{Var}_6^{\text{Gauss}} \simeq 15(180 + 135\sqrt{2} + 8\sqrt{6})\sqrt{\pi}T, & \beta_6 = \frac{1}{30(180+135\sqrt{2}+8\sqrt{6})\sqrt{\pi}}. \end{cases} \quad (19)$$

Again, these calculations are quite straightforward.

B. Large deviations of A_n

The $A_n \rightarrow \infty$ tail of the probability distribution $P(A_n, T) \sim \exp[-S(A_n, T)]$ is dominated by a single *optimal* path, that is the most likely realization of the process $x(t)$ conditioned on a specified value of A_n [6, 12]. The optimal path is the minimizer of the Gaussian action $S[x(t)]$ along paths conditioned on the specified (large) value of A_n . For completeness, here we briefly recap, with slight changes, this calculation [12].

For a stationary Gaussian process the modified action functional to be minimized is the following:

$$S_\lambda[x(t)] = \frac{1}{2} \int_{-\infty}^{\infty} dt \int_{-\infty}^{\infty} dt' K(t-t') x(t) x(t') - \lambda \int_{-\infty}^{\infty} dt x^n(t) [\theta(t) - \theta(t-T)]. \quad (20)$$

The first term in Eq. (20) determines (up to a pre-exponential factor) the statistical weight $P[x(t)] \sim \exp(-S[x(t)])$ of a given realization $x(t)$ of the process, and $K(\dots)$ is the inverse kernel of the stationary Gaussian process, defined

by the relation

$$\int_{-\infty}^{\infty} K(\tau) \kappa(t - \tau) d\tau = \delta(t). \quad (21)$$

The second term in Eq. (20) conditions the process on a large area A_n , see Eq. (1), with λ playing the role of a Lagrange multiplier, and $\theta(\dots)$ denoting the Heaviside step function.

The linear variation of the modified action (20) must vanish, which yields a nonlocal analog of the Euler-Lagrange equation for the optimal path $x(t)$:

$$\int_{-\infty}^{\infty} dt' K(t - t') x(t') = n \lambda x^{n-1}(t) [\theta(t) - \theta(t - T)]. \quad (22)$$

Multiplying both sides of this equation by $\kappa(\tau)$ and using Eq. (21), one arrives at the integral equation [12]

$$x(t) = n \lambda \int_0^T dt' \kappa(t - t') x^{n-1}(t'). \quad (23)$$

Using Eq. (22), one can express the action $S(A_n, T)$ as follows [12]:

$$S(A_n, T) = \frac{1}{2} \int_{-\infty}^{\infty} dt x(t) \int_{-\infty}^{\infty} dt' K(t - t') x(t') = \frac{n \lambda}{2} \int_0^T dt x^n(t) = \frac{n \lambda A_n}{2}, \quad (24)$$

where the Lagrange multiplier $\lambda = \lambda(A_n)$ is to be ultimately determined from Eq. (1).

At $n > 2$ the integral equation (23) is nonlinear, and the ensuing possible multiplicity of solutions plays a crucial role. In particular, an instanton solution emerges, which is localized on the characteristic correlation time scale defined by the covariance function $\kappa(t)$. At sufficiently large T this localized-in-time instanton solution has a lesser action than an almost constant, delocalized solution [which would lead to the standard large-deviation scaling (2)]. The Gaussian action on such an instanton is [12]:

$$S_{\text{inst}}(A_n, T) = c_n A_n^{2/n}, \quad T \rightarrow \infty, \quad (25)$$

where the coefficients c_n are determined by the covariance function $\kappa(t)$ and by n . Equation (25) has the same form as its counterpart for the OU process [6], and it determines the second term in the anomalous rate function (6).

For the standard OU process, the coefficients c_n were found, for all $n > 2$, in Ref. [6] (see also Refs. [12] and [9]):

$$c_n^{\text{OU}} = \frac{n}{4} \left[\frac{2\sqrt{\pi} \Gamma(\frac{n}{n-2})}{(n-2) \Gamma(\frac{3n-2}{2n-4})} \right]^{\frac{n-2}{n}}, \quad n > 2. \quad (26)$$

For the Gaussian covariance $\kappa(t) = \exp(-t^2)$, the coefficients c_n were obtained in Ref. [12]:

$$c_n^{\text{Gauss}} = \frac{(n-1)^{\frac{n-1}{n}}}{2\pi^{\frac{1}{n}} [n(n-2)]^{\frac{n-2}{2n}}}, \quad n > 2. \quad (27)$$

C. Mixed region and DPT

Equations (10) and (25) – for the typical fluctuations and large deviations, respectively – alongside with the T -independence of the coefficients β_n and c_n provide all the ingredients for the validity of the arguments of Ref. [9]. This leads to the anomalous scaling (3), to the large deviation function (5) and (6), and to the first-order DPT at the critical point (8). For completeness we will now briefly reproduce the arguments of Ref. [9]

A crucial realization of Ref. [9] was that there is an intermediate region of *moderately large* deviations of $\Delta A_n = A_n - \langle A_n \rangle$. In this *mixed* region a deviation of the empirical observable ΔA_n can be viewed as the sum of two almost

independent contributions arising on well-separated time scales. The first of them, $\Delta A_{n,\text{inst}}$, comes from an instanton, which is localized on a short time interval $\tau_{\text{inst}} \ll T$ [a characteristic time scale of the covariance $\kappa(t)$]. The second contribution, $\Delta A_n - \Delta A_{n,\text{inst}}$, comes from fluctuations spread uniformly over the remaining time $T - \tau_{\text{inst}}$, and it obeys the central-limit-type Gaussian statistics (10).

Since these two mechanisms act on different time scales and, at $T \rightarrow \infty$, interact only weakly, the probability of observing a specified ΔA_n can be expressed as a convolution of the two separate contributions [9],

$$P(A_n, T) \simeq \int_0^{\Delta A_n} P_{\text{inst}}(\Delta A_{n,\text{inst}}, T) P_{\text{Gauss}}(\Delta A_n - \Delta A_{n,\text{inst}}, T) d\Delta A_{n,\text{inst}}, \quad (28)$$

where the integration is over the instanton contributions. In the large- T limit, this integral is dominated by the saddle-point of the effective joint action, describing the interplay between the typical and large fluctuations:

$$S_{\text{mixed}}(\Delta A_n, \Delta A_{n,\text{inst}}, T) = \frac{\beta_n (\Delta A_n - \Delta A_{n,\text{inst}})^2}{T} + c_n \Delta A_{n,\text{inst}}^{2/n}. \quad (29)$$

The saddle point is located in the region where the two contributions are comparable, that is where $\Delta A_n \sim \Delta A_{n,\text{inst}} \sim T^{n/(2n-2)}$. (This implies that, as T goes to infinity, one should keep $\Delta A_n/T^{n/(2n-2)}$ constant [9]). The saddle-point evaluation yields Eqs. (3)-(6) for the probability distribution and Eq. (8) for the critical point of the first-order DPT [9].

As one can see, the main findings of Ref. [9], obtained for stationary Markov processes, can be directly extended to (in general non-Markovian) *short-correlated* Gaussian processes. In Sec. IV we compare these predictions with replica-exchange Wang-Landau simulations for the Gaussian covariance introduced in Sec. II A 2.

III. LONG-CORRELATED GAUSSIAN PROCESSES

Now let us consider *long-correlated* stationary Gaussian processes $x(t)$ whose covariance exhibits a power-law tail,

$$\kappa(t \rightarrow \infty) \simeq B|t|^{-\alpha}, \quad \alpha > 0. \quad (30)$$

A heavy tail corresponds to $\alpha < 1$. We start with the typical fluctuations of ΔA_n .

A. Typical fluctuations

Since the integrand in Eq. (14) depends only on the difference $t - s$, we can rewrite the double integral as a single integral:

$$\text{Var}_n = \sum_{m=0}^{\lfloor \frac{n-1}{2} \rfloor} \frac{(n!)^2}{(n-2m)!(2^m m!)^2} \kappa^{2m}(0) \int_{-T}^T (T - |t|) \kappa^{n-2m}(t) dt. \quad (31)$$

Each term of the sum with index $p = n - 2m$ involves the integral

$$I_p(T) = \int_{-T}^T (T - |t|) \kappa^p(t) dt. \quad (32)$$

Using the covariance tail asymptotic (30), one can identify three distinct regimes of the large- T scaling behavior of $I_p(T)$, depending on the integrability of the p -th power of the covariance, $\kappa^p(t)$, at $T \rightarrow \infty$:

$$I_p(T) \sim \begin{cases} T^{E_p(\alpha)}, & \text{with } E_p(\alpha) = 2 - p\alpha, \text{ for } p\alpha < 1, \\ T, & \text{for } p\alpha > 1, \\ T \ln T, & \text{for } p\alpha = 1. \end{cases} \quad (33)$$

Since $\alpha > 0$, the exponent $E_p(\alpha)$ decreases with p . Therefore, the dominating contribution to the variance comes from the term with the largest $E_p(\alpha)$ or, equivalently, with the lowest possible index p_{min} in Eq. (31), which is

$$p_{\text{min}} = \begin{cases} 1, & \text{for odd } n, \\ 2, & \text{for even } n. \end{cases} \quad (34)$$

This yields a threshold value $\alpha = \alpha_c$ separating the “normal” regime $\alpha > \alpha_c$, where the variance grows linearly with T , and the regime of an anomalous scaling of the variance with T at $\alpha < \alpha_c$:

$$\alpha_c = \frac{1}{p_{\min}} = \begin{cases} 1, & \text{for odd } n, \\ 1/2, & \text{for even } n. \end{cases} \quad (35)$$

Altogether, we have at $T \rightarrow \infty$:

$$\text{Var}_n \sim \begin{cases} T, & \text{for } \alpha \geq \alpha_c, \\ T^E, & \text{for } \alpha < \alpha_c, \end{cases} \quad \text{where} \quad \alpha_c = \begin{cases} 1, & \text{for odd } n, \\ 1/2, & \text{for even } n, \end{cases} \quad \text{and} \quad E = \begin{cases} 2 - \alpha, & \text{for odd } n, \\ 2 - 2\alpha, & \text{for even } n. \end{cases} \quad (36)$$

Using Eq. (7), we determine the scaling behavior of β_n with T :

$$\beta_n \sim \begin{cases} 1, & \text{for } \alpha \geq \alpha_c, \\ T^{\alpha-1}, & \text{for } \alpha < \alpha_c \text{ and odd } n, \\ T^{2\alpha-1}, & \text{for } \alpha < \alpha_c \text{ and even } n. \end{cases} \quad (37)$$

Importantly, for $\alpha < \alpha_c$, the coefficients β_n depend on T , which reflects a faster-than-linear scaling behavior of the variance with T in this regime.

B. Large deviations

Large deviations of A_n for stationary Gaussian processes with long-range correlations, described by Eq. (30), have been recently studied in Ref. [22] in the particular case of the fractional Ornstein-Uhlenbeck process. Similarly to the short-correlated case, a key factor in determining the large-deviation tail of $P(A_n, T)$ is a competition between localized (instanton-type) and delocalized solutions. The T -independent characteristic duration of the instanton solution, $\tau_{\text{inst}} \ll T$, is determined by the intrinsic time scale of the covariance $\kappa(t)$, and the presence of such a time scale is necessary for the existence of instanton. Further, there is a critical value $\alpha = \alpha(n)$ at which a transition occurs between localized and delocalized solutions of Eq. (23), and correspondingly, between distinct scaling behaviors of the large-deviation action (25).

The action corresponding to a localized solution of Eq. (23) exhibits the same scaling behavior with T , see Eq. (25), as that for the short-correlated case. To estimate the action corresponding to a *delocalized* solution, one can assume that it is almost constant [22]. Then, using the large- t asymptotic of the covariance (30) in Eq. (23) and integrating both sides of the equation over $(0, T)$, we obtain the following order-of-magnitude relation:

$$\text{const}^{(n-2)} \sim T \left(n\lambda \int_0^T \int_0^T \kappa(t-s) dt ds \right)^{-1} \sim \lambda^{-1} B^{-1} T^{\alpha-1}, \quad T \rightarrow \infty. \quad (38)$$

Expressing the corresponding Lagrange multiplier λ through A_n and using Eqs. (20) and (22), we find that the action, associated with an (almost constant) delocalized optimal path, scales as

$$S_{\text{const}} \sim T^{\alpha-2/n} A_n^{2/n}. \quad (39)$$

This action decreases with T for

$$0 < \alpha < \alpha_* \equiv 2/n, \quad (40)$$

making the delocalized solution favorable as $T \rightarrow \infty$. For $\alpha \geq \alpha_*$, a localized solution yields a T -independent action (25) which is therefore optimal. Overall, the scaling behavior of the large-deviation action for long-correlated stationary Gaussian processes is the following:

$$S(A_n, T) = c_n A_n^{2/n}, \quad \text{with} \quad c_n \sim \begin{cases} 1, & \alpha > \alpha_*, \\ T^{\alpha-2/n}, & \alpha < \alpha_*. \end{cases} \quad (41)$$

C. Mixed region

Even when one or both of the coefficients β_n and c_n in Eq. (29) are T -dependent, we can still predict the scaling behavior $\Delta A_n \sim T^\nu$ by balancing in Eq. (29) the instanton contribution $c_n A_n^{2/n}$ with the contribution from the typical, Gaussian fluctuations, $\beta_n A_n^2/T$:

$$c_n T^{2\nu/n} \sim \frac{\beta_n}{T} T^{2\nu}. \quad (42)$$

Combining this relation with the conditions (37) and (41), we identify three distinct scaling regimes for the distribution $P(A_n, T) \sim \exp[-T^\mu f_n(\Delta A_n T^{-\nu})]$.

In the regime $\alpha > \alpha_c$ (that is, for correlation tails which are not heavy or not too heavy, for odd and even n , respectively), both coefficients β_n and c_n are independent of T . In this regime, the probability distribution exhibits the anomalous scaling and the first-order DPT characteristic of the short-correlated processes, as described by Eqs. (3)-(6) for the probability distribution and Eq. (8) for the critical point [9].

In the regime of $\alpha_* \leq \alpha < \alpha_c$, the long-range correlations modify the scaling of the typical fluctuations of A_n , so that the coefficients β_n depend on T . The large deviations, however, are still governed by a localized instanton-like optimal path, so that c_n is T -independent. Therefore, as $T \rightarrow \infty$, the first-order DPT should persist, but it shifts toward larger A_n . Here the anomalous scaling of the probability distribution is described by Eq. (3) with the exponents μ and ν which depend both on n and on α :

$$\mu = \begin{cases} \frac{2(2-\alpha)}{2n-2}, & \text{for odd } n, \\ \frac{2(2-2\alpha)}{2n-2}, & \text{for even } n, \end{cases} \quad \nu = \begin{cases} \frac{n(2-\alpha)}{2n-2}, & \text{for odd } n, \\ \frac{n(2-2\alpha)}{2n-2}, & \text{for even } n. \end{cases} \quad (43)$$

In the regime of very long correlations, $\alpha < \alpha_*$, both β_n and c_n are T -dependent. Here large but almost uniform deviations in time have a lower action cost than localized instantons. Consequently, the convolution construction (28) does not apply, and a DPT is absent. The system therefore should exhibit a smooth crossover between the typical and large fluctuations. The crossover is expected to occur at $\Delta A_n \sim T^\nu$, where the Gaussian action of the typical fluctuations is comparable with the action corresponding to a delocalized optimal path which determines the large deviations of A_n , and we obtain Eq. (3) with

$$\mu = \begin{cases} \alpha, & \text{for odd } n, \\ \frac{n-2}{n-1}\alpha, & \text{for even } n, \end{cases} \quad \nu = \begin{cases} 1, & \text{for odd } n, \\ 1 - \frac{n\alpha}{2n-2}, & \text{for even } n, \end{cases} \quad (44)$$

and $f_n(y) \sim \mathcal{O}(1)$ is a smooth function of y .

The resulting phase diagram on the (α, n) plane, shown in Fig. 1, describes three distinct regimes of the anomalous scaling of the distribution $P(A_n, T) \simeq \exp[-T^\mu f_n(\Delta A_n T^{-\nu})]$. The corresponding values of the exponents μ and ν are presented in Table I.

TABLE I. Anomalous scaling behavior of $P(A_n, T) \simeq \exp[-T^\mu f_n(\Delta A_n T^{-\nu})]$ for stationary Gaussian processes with long-ranged correlations, $\kappa(t \rightarrow \infty) \simeq B|t|^{-\alpha}$ at $|t| \rightarrow \infty$. The two critical exponents, α_c from Eq. (35) and $\alpha_* = 2/n$, separate three distinct scaling regimes.

α	μ and ν	Behavior of $f_n(y)$
$\alpha > \alpha_c$	$\mu = \frac{2}{2n-2}, \quad \nu = \frac{n}{2n-2}$	nonanalytic
$\alpha_* \leq \alpha < \alpha_c$	Odd n : $\mu = \frac{2(2-\alpha)}{2n-2}, \quad \nu = \frac{n(2-\alpha)}{2n-2}$ Even n : $\mu = -\frac{2(2-2\alpha)}{2n-2}, \quad \nu = -\frac{n(2-2\alpha)}{2n-2}$	nonanalytic
$0 < \alpha < \alpha_*$	Odd n : $\mu = \alpha, \quad \nu = 1$ Even n : $\mu = \frac{n-2}{n-1}\alpha, \quad \nu = 1 - \frac{n\alpha}{2(n-1)}$	analytic

Interestingly, for $n = 4$ the critical exponents α_* and α_c coincide: $\alpha_* = \alpha_c = 1/2$. As a result, there is no yellow region in this case.

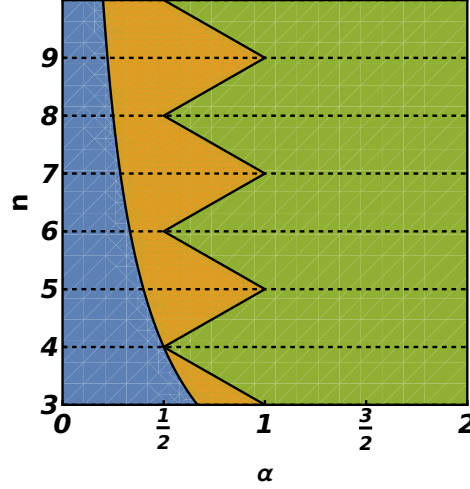


FIG. 1. Phase diagram of the anomalous scaling behavior of the distribution $P(A_n, T) \simeq \exp[-T^\mu f_n(\Delta A_n T^{-\nu})]$ for $n > 2$ on the (α, n) plane. Different colors correspond to regions with a different behavior of the scaling exponents μ and ν . The green region represents the effectively short-correlated regime $\alpha > \alpha_c$, where the rate function $f_n(y)$ exhibits a first-order DPT identified in Ref. [9]. The yellow region corresponds to the moderately correlated regime with $\alpha_* \leq \alpha < \alpha_c$, which also displays a first-order DPT, but with a different behavior of μ and ν . The blue region corresponds to the long-correlated regime $\alpha < \alpha_*$, where the rate function $f_n(y)$ is analytic. For illustrative purposes we have extended the phase diagram to non-integer n , but the results are applicable only for integer $n > 2$, as indicated by the dashed lines.

D. fOU process

A representative example of a stationary Gaussian process with a power-law asymptotic behavior of the correlation is provided by the fractional Ornstein–Uhlenbeck (fOU) process [19, 20], which has recently attracted a renewed attention in the context of large deviations [22, 23]. The fOU process is governed by the linear overdamped Langevin equation :

$$\dot{x}(t) + \gamma x = \sqrt{2D}\xi(t), \quad (45)$$

where $D > 0$ is the coefficient of fractional diffusion, and $\xi(t)$ is the fractional Gaussian noise: a centered stationary Gaussian process with the covariance

$$c(\tau) = \langle \xi(t + \tau)\xi(t) \rangle = \frac{d}{d\tau}(H|\tau|^{2H-1}\text{sgn}(\tau)) = \frac{1}{2} \frac{d^2}{d\tau^2} |\tau|^{2H}, \quad (46)$$

where $0 < H < 1$ is the Hurst exponent. The covariance $\kappa(\tau) = \langle x(t + \tau)x(t) \rangle$ of the stationary fOU process is given by

$$\kappa(\tau) = \frac{1}{2\pi} \int_{-\infty}^{\infty} \kappa_\omega e^{-i\omega\tau} d\omega = \frac{D\Gamma(2H+1)}{\gamma^{2H}} \left[\cosh(\gamma\tau) - \frac{|\gamma\tau|^{2H}}{\Gamma(2H+1)} {}_1F_2\left(1; H + \frac{1}{2}, H + 1; \frac{\tau^2\gamma^2}{4}\right) \right], \quad (47)$$

where ${}_1F_2(\dots)$ is the hypergeometric function [24]. At long times this covariance exhibits a power-law tail

$$\kappa(|t| \rightarrow \infty) \simeq \frac{2DH(2H-1)}{\gamma^2} |t|^{-(2-2H)}, \quad (48)$$

which corresponds to $\alpha = 2 - 2H$ in Eq. (30). With this α , Eqs. (35) and (40) yield the critical values H_c and H_* which separate the regimes of the ordinary and the anomalous *typical* fluctuations, and of the localized and delocalized optimal paths, respectively:

$$H_c = \begin{cases} 1/2, & \text{for odd } n, \\ 3/4, & \text{for even } n, \end{cases} \quad \text{and} \quad H_* = 1 - 1/n. \quad (49)$$

For general H the integral, which appears in Eq. (31) for the variance of A_n , can be evaluated numerically. The calculation of the coefficients c_n , which describe the large deviations, can be done via an iterative numerical solution of the nonlinear integral equation (22), see Sec. IV A. As an example, Table II presents the numerically obtained T -independent coefficients β_3 and c_3 , and the predicted values of the DPT point y_c , for $n = 3$ and $H = 1/4$. (For convenience, here we are using the units where $D = \frac{\gamma^{2H}}{\Gamma(2H+1)}$ and $\gamma = 1$.) The T -dependent coefficients (β_3 for $H = 3/5$, and both β_3 and c_3 for $H = 3/4$) were obtained by fitting numerically the computed values of c_3 and β_3 by the power-law functions $\beta_3 = \tilde{\beta}_3 T^{1-2H}$ and $c_3 = \tilde{c}_3 T^{1-2H-2/n}$, respectively, over a range of T from 10^2 to $4 \cdot 10^3$.

TABLE II. Numerically computed coefficients β_3 and c_3 for the fOU process with different H .

H	β_3	c_3	y_3
1/4	0.095	0.751	4.134
3/5	$0.028T^{-1/5}$	0.363	5.999
3/4	$0.036T^{-1/2}$	$0.332T^{-1/6}$	—

Figure 2 shows the phase diagram of the fOU process in the (H, n) plane. The critical Hurst exponents H_c and H_* define three distinct regions in the (H, n) plane. These regions determine the scaling exponents μ and ν of the asymptotic distribution (3) in the large T limit, see Table III. To remind the reader, for $n = 4$ the yellow region is absent.

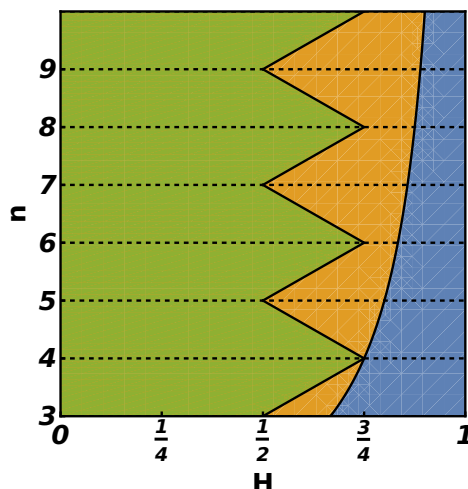


FIG. 2. Phase diagram of the anomalous scaling behavior of the distribution $P(A_n, T)$ for $n > 2$ on the (H, n) plane. Different colors correspond to regions with a different behavior of the scaling exponents μ and ν . The green region represents the short-correlated regime $H \leq H_c$, where the rate function exhibits a first-order DPT. The yellow region corresponds to the moderately correlated regime with $H_* \geq H > H_c$, which also displays a first-order DPT, but with a different behavior of μ and ν . The blue region corresponds to the long-correlated regime $H > H_*$, where the DPT disappears. For illustrative purposes, we have extended the phase diagram to non-integer n , but the results are applicable only for integer $n > 2$, as indicated by the dashed lines.

IV. LARGE DEVIATION SIMULATIONS

A. Replica-Exchange Wang-Landau Simulations

The predicted DPT can be observed only at very large T which are inaccessible to conventional Monte-Carlo simulations. Therefore, we employed the Replica-Exchange Wang-Landau (REWL) algorithm [25–27] to probe the probability density $P(A_n, T)$ and to sample discretized configurations of stationary Gaussian processes. The essence of

TABLE III. Fluctuation regimes and scaling behaviors for the fOU process. The critical exponents H_c and $H_* = 1 - 1/n$ separate three distinct regimes corresponding to different scaling and large-deviation behaviors of $P(A_n, T)$.

H	μ and ν	Behavior of $f_n(y)$
$H \leq H_c$	$\mu = \frac{2}{2n-2}, \quad \nu = \frac{n}{2n-2}$	nonanalytic
$H_c < H \leq H_*$	Odd n : $\mu = \frac{4H}{2n-2}, \quad \nu = \frac{2nH}{2n-2}$ Even n : $\mu = \frac{4(2H-1)}{2n-2}, \quad \nu = \frac{2n(2H-1)}{2n-2}$	nonanalytic
$H > H_*$	Odd n : $\mu = 2 - 2H, \quad \nu = 1$ Even n : $\mu = \frac{n-2}{n-1}(2-2H), \quad \nu = 1 + \frac{n(2H+2)}{2(n-1)}$	analytic

the REWL approach lies in dividing the target space of A_n into multiple smaller overlapping windows. Every window runs one or more replicas. Each replica carries out an ordinary Wang–Landau (WL) sampling process [28, 29] with its own histogram and density of states within the corresponding window. After a fixed number of Wang–Landau steps, replica exchanges between the overlapping windows are performed. The probability of accepting a replica exchange, $P(X \leftrightarrow Y)$, of configurations X and Y between the windows i and j is given by

$$P(X \leftrightarrow Y) = \min \left[1, \frac{S_i(A_X)S_j(A_Y)}{S_i(A_Y)S_j(A_X)} \right], \quad (50)$$

where $S_i(A_X)$ is the current estimator for the density of states, $S(A_X, T) = -\ln P(A_X, T)$, in the window i , for the value $A_X = \int_0^T X^n(t)dt$ corresponding to its configuration X . Once the simulation is complete, i.e. when the slowest replica reaches the desired precision, the overlapping fragments of the density of states are merged by appropriately shifting adjacent segments [27].

The WL simulations were performed by discretizing the continuous process $X(t)$ over a large but finite domain $(0, T_D]$. The discretization is represented as $\vec{X} = (X(\Delta t), \dots, X(T_D))$, where Δt is the lattice step, and $L \equiv T_D/\Delta t \gg 1$ is the duration of the discretized trajectory. The dynamical observable A_n of the discretized process \vec{X} is approximated by the discrete sum

$$A_n = \Delta t \sum_{k=L/2-T/2\Delta t}^{L/2+T/2\Delta t} X^n(k\Delta t). \quad (51)$$

Since a direct sampling of Gaussian stationary processes is computationally expensive, we employed the Circulant Embedding Method (CEM) [30, 31], which enables sample generation in $O(L \ln L)$ time. For more details on the WL simulations of stationary Gaussian processes see Ref. [32], where the CEM and the WL algorithm were used to study the large deviations of the potential barrier height distribution of statistically homogeneous Gaussian disorder potentials.

An important issue in these simulations is a proper choice of the lattice step Δt to resolve the instanton-like optimal paths of $X(t)$ and accurately measure the corresponding action. To address this issue, we solved numerically, by a straightforward iteration procedure, a discretized version of the integral equation (23) which describes the optimal paths in the limit of large A_n :

$$y_i(m\Delta t) = \Delta t \sum_{k=L/2-T/2\Delta t}^{L/2+T/2\Delta t} \kappa((m-k)\Delta t) y_{i-1}^{n-1}(k\Delta t), \quad (52)$$

where $y(t) = (n\lambda)^{1/(n-2)}x(t)$ is the rescaled optimal path. Similarly to Ref. [22], we reduced the discretization step Δt until the numerical solution $y(t)$ converged with a required accuracy. Then we calculated the action $S(A_n, T)$ of the optimal path, leading to a discrete approximation of c_3 . Additional details of the numerical implementation of the iteration process are presented in the Appendix of Ref. [22].

We checked that for $\Delta t < 1.0$ the discrete approximation of the coefficient c_3 for the Gaussian covariance $\kappa(t) = \exp(-t^2)$ closely matches the exact analytical value given in Eq. (27). In the REWL simulations of this case we used $\Delta t = 0.5$, resulting in a relative discretization error of the order of 10^{-11} .

The REWL simulations ran for several integration times: $T = 500, 1000, 2000, 4000$, and 8000 . The duration of the continuous trajectories – $T_D = 512, 1024, 2048, 4096$, and 8192 , respectively – were chosen to be large enough to minimize the edge effects in the integration region while still be manageable for an effective sampling. (The durations of the discretized trajectory were chosen to be powers of 2 to optimize the FFT efficiency.)

Finally, the parameters D and γ were chosen to be $D = \frac{\gamma^{2H}}{\Gamma(2H+1)}$ and $\gamma = 1$, while the discretization step Δt was kept the same as for the Gaussian-correlated process. Following recommendations of Ref. [26], the overlap between the windows for all replicas in the simulations was set to 75%.

B. Theory versus simulations

We now present the numerical results for $n = 3$ for the Gaussian-correlated process, as an example of short-correlated Gaussian processes, and for the fOU process – a process which interpolates between the short- and intermediately-correlated regimes, which exhibit the first-order DPTs, and the long-correlated regime with a smooth crossover between the Gaussian fluctuations and the large deviations.

1. Gaussian covariance

Combining Eqs. (8), (19) and (27), obtained for the process with the Gaussian covariance $\kappa(t) = \exp(-t^2)$, we determine the critical point of the first-order DPT for $n = 3$: $y_c \simeq 8.28$. Our simulation results for the rescaled action $-T^{-1/2} \ln P(A_3, T)$ are shown in the left panel of Fig. 3 along with the theoretically predicted behavior, see Eqs. (5) and (6). The black lines correspond to the Gaussian approximation $b_3 y^2$ for $y < y_c$ and to the mixed scenario for $y > y_c$, the red dots mark the predicted critical point y_c and the finite discontinuity of the first derivative at $T \rightarrow \infty$.

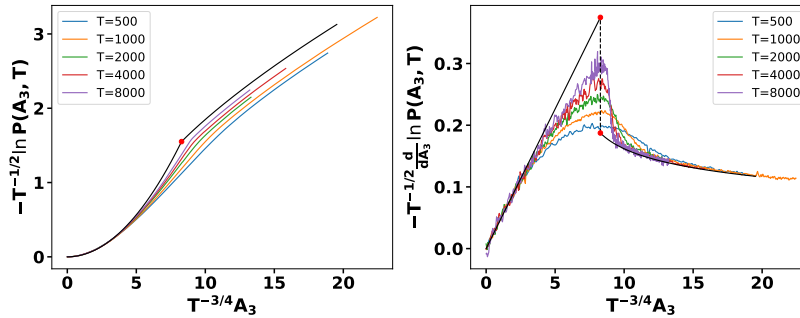


FIG. 3. The emerging first-order DPT for the Gaussian covariance. Left: the large- T behavior of the rescaled action, $-T^{-1/2} \ln P(A_3, T)$, as measured in the REWL simulations for a set of values of $T \gg 1$ marked by different colors. Right: the first derivative of the rescaled action with respect to A_3 . The red dots mark the predicted critical point y_c (left) and the finite discontinuity of the derivative (right).

2. fOU process

The simulation results for the rescaled action $-T^{-\mu} \ln P(A_3, T)$ of the fOU process for a set of Hurst exponents H are shown in Fig. 4a-d along with the predicted behavior, see Table III. For completeness, this set includes the important case $H = 1/2$ (the standard OU process), for which the theoretical predictions [6, 9] have so far not been tested numerically. The black lines correspond to Eqs. (5) and (6) with the parameters β_3 and c_3 given in Table II. In the short-correlated regime (Fig. 4a,b), corresponding to $H = 1/4$ and $H = 1/2$, the scaling exponents (μ, ν) are universal and independent of the details of the covariance function. For $H = 3/5$ the covariance tail of the fOU process is sufficiently long-correlated to affect the typical fluctuation scaling, see Eq. (31) and Table II. Here the scaling behavior of the action $-\ln P(A_3, T)$ becomes H -dependent (see Table III for $H_* \geq H > H_c$). The black lines in Fig. 4 represent the Gaussian approximation $\tilde{b}_3 y^2$ for $y < y_c$ and, in Figs. a-c, the supercritical asymptotic $c_3 y^{2/3}$ for $y > y_c$,

with the coefficients \tilde{b}_3 and c_3 given in Table II. Here $\tilde{\beta}_3 = \beta_3 T^{2H-1}$ is T -independent. In the strongly-correlated case $H = 3/4$, presented in Fig. 4d, the DPT disappears completely – again, as predicted by the theory. Instead, a smooth crossover is observed between the typical fluctuations, described by the Gaussian asymptotic $\beta_3 y^2$, and the large deviations, described by the asymptotic $\tilde{c}_3 y^{2/3}$.

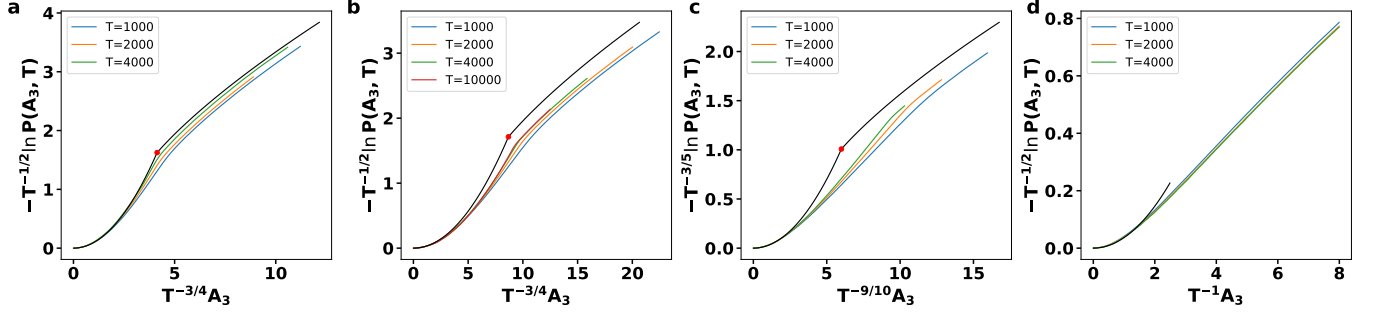


FIG. 4. The large- T behavior of the rescaled action, $-T^{-\mu} \ln P(A_3, T)$, as measured in the REWL simulations of the fOU process for several values of T (marked by different colors) and a set of Hurst exponents H : a) $H = 1/4$; b) $H = 1/2$; c) $H = 3/5$, and d) $H = 3/4$. The red dots mark the predicted critical point y_c .

One can see from Figs. 3 and 4 that, as T increases, the simulation results slowly converge toward the analytical predictions, and the DPT in the panels a-c becomes more pronounced. The convergence is better seen in the plots of the numerical derivative of the rescaled simulated actions with respect to A_3 , shown in the right panel of Fig. 3 and in Fig. 5. The derivative plots highlight a gradual sharpening of the transition with an increase of T and confirms the anomalous scaling exponents characterizing the emerging DPT.

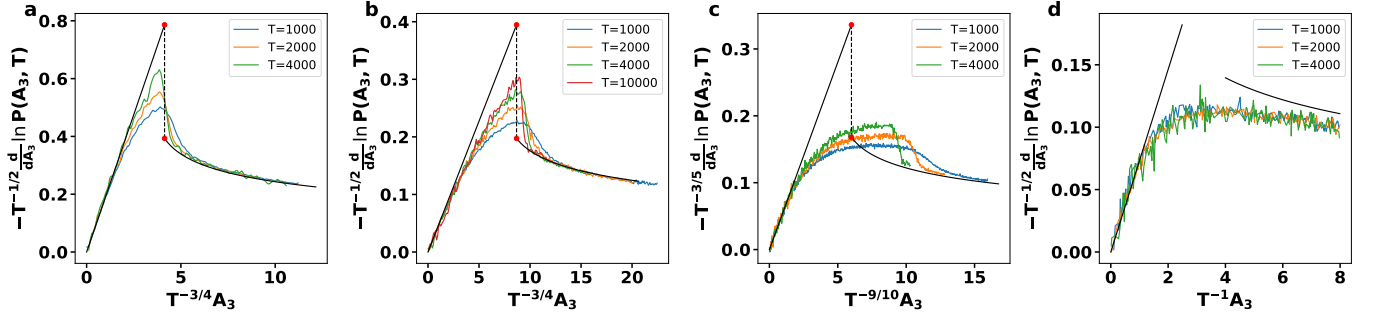


FIG. 5. The first derivative of the rescaled action, measured in the REWL simulations, with respect to A_3 for different Hurst exponents H : a) $H = 1/4$; b) $H = 1/2$; c) $H = 3/5$, and d) $H = 3/4$. The red dots in the panels a-c mark the finite discontinuity of the derivative.

3. Optimal paths

We also sampled, in the REWL simulations, individual realizations of the fOU process $x(t)$ conditioned on different values of A_3 in the mixed region above the predicted phase transition. Examples of such realizations, clearly showing instanton configurations, are presented in Fig. 6. The black curves represent the sampled trajectories, arbitrarily shifted in time such that the instanton maxima are positioned at $t = 0$. The blue lines show the ensemble-averaged trajectories. The red dashed lines represent the optimal paths obtained by the numerical solution of the nonlinear integral equation (23), as explained in Sec. IV A. In the mixed scenario with a DPT, that is for $H = 1/4$, $H = 1/2$, and $H = 3/5$, the optimal paths correspond to the instanton contribution, given by the minimizer $z_*(y)$ of Eq. (6). As one can see from Fig. 6, the instanton, which gives the predicted contribution to the rate function, agrees well with the ensemble-averaged trajectory. For $H = 3/4$ the optimal path is delocalized, and the measured trajectories are plotted without any shifts. In this case the optimal path corresponds to the value of A_3^{deloc} matching that of the ensemble-averaged trajectory $A_3^{\text{deloc}} = \int_0^T \langle x \rangle_{\text{ens}}^3(t) dt$.

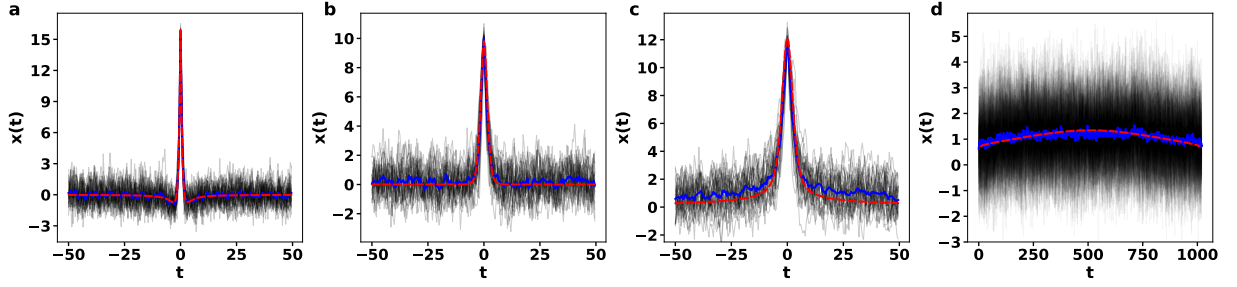


FIG. 6. N realizations of the fOU process $x(t)$ conditioned on A_3 for $T = 10^3$ (the black lines). The blue lines correspond to the trajectories averaged over the N realizations. The red dashed lines show theoretically predicted optimal paths. Panel a: $H = 1/4$, $N = 30$, $A_3 = yT^{3/4}$ for $y = 15$. Panel b: $H = 1/2$, $N = 30$, $A_3 = yT^{3/4}$ for $y = 15$. Panel c: $H = 3/5$, $N = 30$, $A_3 = yT^{9/10}$ for $y = 5$. Panel d: $H = 3/4$, $N = 100$, $A_3 = yT$ for $y = 8$.

In addition to the instanton contribution to A_3 , we also examined the non-instanton part, coming from the fluctuations uniformly distributed along the trajectory. Specifically, we computed the dynamical observable itself at intermediate times $0 \leq t \leq T$:

$$A_3(t) = \int_0^t x_{\text{uniform}}(s)^3 ds, \quad (53)$$

where each trajectory $x_{\text{uniform}}(s)$ is obtained by subtracting the corresponding measured optimal path (shown in Fig. 6) from the sampled trajectory $x(s)$, and the optimal path is aligned with the instanton maxima location of the trajectory. The black curves in Fig. 7 represent the dynamical observables $A_3(t)$ at intermediate times, calculated using the same ensemble of trajectories as in Fig. 6. The blue lines show the ensemble-averaged values of $A_3(t)$. The red lines represent the theoretically predicted uniform contribution $A_3 - A_{3,\text{inst}}$. As one can see, a better agreement between the theoretical and simulated slopes, and between the theoretical optimal paths and the sampled instanton configurations in Fig. 6, is observed for smaller H . This observation, which is to be expected, correlates with the fact that a faster convergence of the simulated action to the theoretical one in Figs. 3 and 4 is also observed for smaller H .

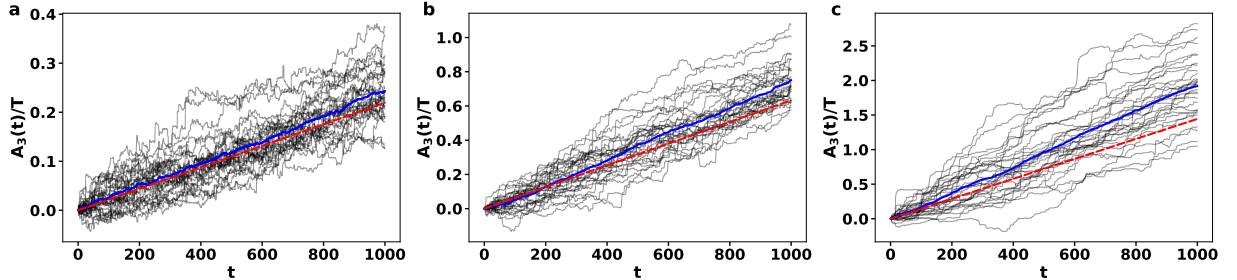


FIG. 7. $N = 30$ realizations of $A_3(t)$. The blue lines correspond to the trajectories averaged over the N realizations. The red dashed lines show the theoretically predicted uniform contributions for: a) $H = 1/4$, $A_3 = yT^{3/4}$ for $y = 15$; b) $H = 1/2$, $A_3 = yT^{3/4}$ for $y = 15$; and c) $H = 3/5$, $A_3 = yT^{9/10}$ for $y = 15$.

V. SUMMARY AND DISCUSSION

As can be seen from the phase diagrams, shown in Figs. 1 and 2, the long-time large-deviation statistics of A_n , $n > 2$, of stationary Gaussian processes are strongly affected by the correlation properties of the process or, more precisely, by the long-time behavior of the autocovariance $\kappa(t)$. Not very surprisingly, all short-correlated Gaussian processes behave in this respect very similarly to the previously studied Ornstein-Uhlenbeck process [9]. That is, their probability densities $P(A_n, T)$ share the same anomalous scaling behavior and the same type of the first-order DPT in the limit of $T \rightarrow \infty$.

Gaussian processes with longer correlations behave differently, and the differences grow as the correlations become more long-ranged. For sufficiently heavy correlation tails the large-deviation function of A_n becomes smooth: no DPT is observed in the limit of $T \rightarrow \infty$. The reason for the analytical behavior of the rate function in this regime is the non-existence of strongly localized solutions for the optimal paths of the process conditioned on large A_n .

Remarkably, there is also an intermediate region of moderately-correlated processes. Here a first-order DPT is present at $T \rightarrow \infty$. The long-time scaling behavior of $P(A_n, T)$, however is different in this case from that for the short-correlated processes, as it explicitly depends on the exponent of the power-law decay of $\kappa(t)$ at $t \rightarrow \infty$. The key factor behind the new scaling regime is the effect of long correlations on the typical, Gaussian fluctuations of A_n .

The localized-in-time instanton-like optimal path, which plays a crucial role in the anomalous scaling and the condensation transition, is qualitatively similar to the “big jump” which dominates the far tail of the distribution $P(S_N, N)$ of the sum $S_N = \sum_{i=1}^N y_i$ of independent identically distributed random variables y_i in the large- N limit. The big-jump principle (BJP) states that, for subexponential tails of the distribution of the random variables, $-\ln P(y_i \rightarrow \infty) \sim y_i^\epsilon$ with $0 < \epsilon < 1$, the distribution tail of the S_N is asymptotically dominated by the single largest summand [33–36]. Discretizing the time integral in Eq. (1), one finds that, at $n > 2$, the (correlated!) random variables $y_i \equiv x_i^n$ in our problem do have a subexponential tail with the power $\epsilon = 2/n < 1$. Therefore, one can expect that, for short-correlated processes, the BJP must hold. Essentially, we have shown here that this is indeed what happens, and have also examined what happens when the correlations increase until the BJP breaks down.

Acknowledgment. We are very grateful to Naftali R. Smith for his insightful advice and suggestions. This research was supported by the Israel Science Foundation (Grant No. 1579/25). A.V. is supported by Instituto Balseiro and by a Simons Foundation Targeted Grant to Institutions.

-
- [1] H. Touchette, Phys. Rep. **478**, 1 (2009).
 - [2] Y. Oono, Prog. Theor. Phys. Suppl. **99**, 165 (1989).
 - [3] A. Dembo and O. Zeitouni, *Large Deviations Techniques and Applications*, 2nd ed. (Springer, New York, 1998).
 - [4] F. den Hollander, *Large Deviations*, Fields Institute Monographs, vol. 14 (AMS, Providence, Rhode Island, 2000).
 - [5] H. Touchette, Physica A **504**, 5 (2018).
 - [6] D. Nickelsen and H. Touchette, Phys. Rev. Lett. **121**, 090602 (2018).
 - [7] F. den Hollander, S.N. Majumdar, J. M. Meylahn, and H. Touchette, J. Phys. A: Math. Theor. **52**, 175001 (2019).
 - [8] J. du Buisson and H. Touchette, Phys. Rev. E **102**, 012148 (2020).
 - [9] N. R. Smith, Phys. Rev. E **105**, 014120 (2022).
 - [10] G. E. Uhlenbeck and L. Ornstein, Phys. Rev. **36**, 823 (1930).
 - [11] A. Bassanoni, A. Vezzani, E. Barkai, and R. Burioni, J. Stat. Mech. (2025) 043201.
 - [12] B. Meerson, Phys. Rev. E **100**, 042135 (2019).
 - [13] D. Nickelsen and H. Touchette, Phys. Rev. E **105**, 064102 (2022).
 - [14] F. Brosset, T. Klein, A. Lagnoux and P. Petit, arXiv:2007.08164.
 - [15] F. Mori, P. Le Doussal, S. N. Majumdar and G. Schehr, Phys. Rev. E **103**, 062134 (2021).
 - [16] F. Mori, G. Gradenigo, S. N. Majumdar, J. Stat. Mech. (2021) 103208.
 - [17] N. R. Smith and S.N. Majumdar, J. Stat. Mech. (2022) 053212.
 - [18] N. R. Smith, Physica A **650** (2024) 129987.
 - [19] P. Cheredito, H. Kawaguchi, and M. Maejima, Electron. J. Probab. **8**, 1 (2003).
 - [20] T. Kaarakka, *Fractional Ornstein-Uhlenbeck Processes* (Tampere University of Technology, Tampere, 2015).
 - [21] R. J. Adler, J. E. Taylor, *Random Fields and Geometry* (Springer-Verlag, New York, 2007).
 - [22] A. Valov and B. Meerson, J. Phys. A: Math. Theor. **58**, 095002 (2025).
 - [23] B. Meerson and P. V. Sasorov, J. Phys. A: Math. Theor. **57**, 445002 (2024).
 - [24] Wolfram Research 2024 Inc., Mathematica Version 14.0.0.0.
 - [25] T. Vogel, Y. W. Li, T. Wüst and D. P. Landau, Phys. Rev. Lett. **110**, 210603 (2013).
 - [26] T. Vogel, Y. W. Li, T. Wüst and D. P. Landau, Phys. Rev. E **90**, 023302 (2014).
 - [27] T. Vogel, Y. W. Li, and D. P. Landau, J. Phys.: Conf. Ser. **1012**, 012003 (2018).
 - [28] F. Wang and D. P. Landau, Phys. Rev. Lett. **86**, 2050 (2001).
 - [29] F. Wang and D. P. Landau, Phys. Rev. E **64**, 056101 (2001).
 - [30] G. Chan and A. T. A. Wood, J. Comput. Graph. Stat., **3**, 409 (1994).
 - [31] C. R. Dietrich and G. N. Newsam, SIAM J. Sci. Comput. **18**, 1088 (1997).
 - [32] A. Valov, N. Levi, and B. Meerson, Phys. Rev. E **110**, 024138 (2024).
 - [33] A. V. Nagaev, Ann. Probab. **7**, 745 (1979).
 - [34] V. V. Petrov, *Sums of Independent Random Variables* (Springer, Berlin, 1975).
 - [35] D. Denisov, A. B. Dieker, and V. Shneer, Ann. Probab. **36**, 1946 (2008).
 - [36] A. Vezzani, E. Barkai, and R. Burioni, Phys. Rev. E **100**, 012108 (2019).